Ab initio study of ground-state properties of the Laves-phase compound $ZrMn_2$

Xing-Qiu Chen,[1] W. Wolf,[2] R. Podloucky,[1] P. Rogl,[1] and M. Marsman[3]
[1]*Institut für Physikalische Chemie, Universität Wien, Liechtensteinstrasse 22A, A-1090, Vienna, Austria*
[2]*Materials Design s.a.r.l., 44, av. F. -A. Bartholdi, 72000 Le Mans, France*
[3]*Institut für Materialphysik, Universität Wien, Sensengasse 8, A-1090, Vienna, Austria*
(Received 15 April 2005; published 25 August 2005)

By an *ab initio* density functional approach the structural and phase stability, electronic and magnetic properties, elastic constants, phonon dispersion, and defect formation of the Laves-phase compound $ZrMn_2$ for the C15, C14, and C36 crystal structures were investigated. In order to study the stability of magnetic phases, nonmagnetic and spin polarized calculations for ferro- and antiferromagnetic orderings were performed. At low temperatures, the ferromagnetic cubic C15 phase was obtained as the ground state, with the ferromagnetic hexagonal C14 and C36 phases being almost degenerate in energy. From the calculated temperature-dependent free energies a structural transformation from C15 to C14 at about $T_{tr}=200$ K is predicted, confirming the experimentally observed C14 structure at elevated temperatures. Elastic properties were investigated for the nonmagnetic and ferromagnetic C14 and C15 phases. Structural stability studies based on the calculated temperature-dependent free vibrational energies very strongly favor the existence of ferromagnetic phases. Point defect formation properties for vacancies and antiste defects were calculated by combining a supercell approach with a statistical mechanics model. Mn antisites are the most favorable defects broadening the homogeneity range of the $ZrMn_2$ phase toward the Mn-rich side. The existence of ordered Mn-rich compounds is predicted. Large magnetic moment of 3 μ_B for Mn antisite defects are derived.

DOI: 10.1103/PhysRevB.72.054440 PACS number(s): 75.50.−y, 61.50.Lt, 63.20.−e, 71.15.Nc

I. INTRODUCTION

A number of experimental studies[1–10] found that $ZrMn_2$ crystallizes in the hexagonal C14 structure at temperatures above 870 K and up to the melting point of 1723 K. Early magnetization and paramagnetic susceptibility measurements[11] yielded a large effective magnetic moment of 2.4 μ_B per Mn atom. Jacob *et al.*[12] hinted that $ZrMn_2$ undergoes a possible magnetic transition at low temperatures. There are, however, no recent experimental reports about the magnetic properties of $ZrMn_2$.

Calculations of the electronic structure have been performed for the hexagonal C14 as well as cubic C15 structure. Based on results of a Korringa-Kohn-Rostoker approach Ishida *et al.*[13] concluded that for the C14 structure Mn atoms at the 2*a* lattice sites might carry a moment and be ferromagnetically ordered. From linearized muffin tin orbitals calculations Asano and Ishido[14] drew the same conclusion, but they also pointed out that according to their results for the C14 structure the ferromagnetic and nonspin polarized states are degenerate in energy. Employing a cluster method Matsumura *et al.*[15] calculated the electronic structure of hydrogenated $ZrMn_2$ containing various alloying elements. Applying a tight-binding approach, H. Yamada[16] reviewed the electronic structure and magnetic properties of the transition metal Laves compounds with the cubic C15 type. However, $ZrMn_2$ was not discussed. Rather recently, by a full-potential linearized augmented plane wave method Hong and Fu[17] studied clean and hydrogenated $ZrMn_2$ (among other compounds) for both the C14 and the C15 structure. For both structures they derived ferromagnetic ordering. However, no information is provided about which structure is the most stable one.

Very recently, by application of the *Vienna ab initio* simulation package (VASP) for $ZrMn_2$ at low temperatures[18] we proposed a peculiar energetical degeneracy of the ferromagnetic phases with C14, C15, and C36 structures claiming that $ZrMn_2$ might be a polymorphic material. We found that at $T=0$ K the C15 structure is slightly more stable than the C14 and C36 structures, but—based on calculated phonon free energies—we predicted a structural phase transition from C15 to C14 at about 160 K. Furthermore, our results on some antiferromagnetically ordered phases showed that these phases are energetically rather close to the ferromagnetic results. So far, no experimental evidence could be found for the stabilization of the C15 structure at low temperatures.

Very important for the ground-state properties of $ZrMn_2$ are its defect properties. The phase diagram[2] exhibits a wide homogeneity range toward the Mn-rich side which is suggested to be due to antisite Mn atoms.[6] The experimental results on the solubility ranges[3–5,9] show rather large variations indicating the problem of fabricating well-defined samples. In particular, magnetic properties could be strongly influenced by the sizeable off-stoichiometry as indeed we will derive from our *ab initio* results.

Summarizing, up to now the magnetic and structural ground-state properties of $ZrMn_2$ at lower temperatures are still unresolved. Therefore, a thorough and detailed *ab initio* density functional study seems to be needed. In our present paper we discuss structural stabilities in connection with magnetic ordering, for ferromagnetic as well as some antiferromagnetic cases, for the C14, C15, and C36 crystal structures (Sec. III). Results for elastic properties (Sec. V) are presented and the electronic structures (Sec. IV) are discussed. Furthermore, for the nonmagnetic and ferromagnetic phases with C14 and C15 structure phonon dispersions and vibrational free energies were calculated in order, again, to understand the influence of magnetism on the structural sta-

bility, now as a function of temperature (Sec. VI). Finally, for studying properties of point defects such as vacancies and antisite atoms in the C14 and C15 structures we applied a combination of supercell calculations and a statistical mechanics model (Sec. VII).

Very recently, by the same techniques as applied for the present work we studied the nonmagnetic Laves-phase compounds $TiCr_2, ZrCr_2$, and $HfCr_2$.[19]

II. COMPUTATIONAL DETAILS

We applied the Vienna *ab initio* simulation package (VASP)[20] with the projector augmented wave potential (PAW)[21,22] construction. An overall energy cutoff of 400 eV was chosen. For Mn the semicore $3p$ states and for Zr the semicore $4s$ and $4p$ states were treated as valence states. For the exchange-correlation functional of our applied density functional (DFT) approach we made use of the generalized gradient approximation[23] (GGA) including the approach of Vosko, Wilk, and Nusair[24] for spin polarized systems. Brillouin-zone integrations were performed on suitable grids of special $\vec{k}$ points according to Monkhorst and Pack[25] ($7\times7\times7$ for C15, $10\times10\times8$ for C14, and $5\times5\times3$ for C36). Full relaxation of geometrical parameters (atomic positions as well as all lattice parameters) was achieved by minimizing forces, stress tensor components, and total energies.

In addition to nonmagnetic (NM) and ferromagnetic (FM) calculations some selected antiferromagnetic cases were studied: For the C14 structure we chose three layerwise antiferromagnetic *initial* arrangements, which are frequently observed by experiment (for illustration see Fig. 2): AF1 (alternating up/down arrangement at $2a/6h$ sites); AF2 (as shown by Fig. 2); AF3 (like in Fig. 2 but up/up and down/down arrangement for subsequent $2a/6h$ layers). The C15 antiferromagnetic structure was modeled according to Nakamura, Metoki, Suzuki, Takayanagi, and Shiga[26] as proposed for YMn_2. For C36 we started the antiferromagnetic calculations by the magnetic moment distribution as shown in Fig. 2.

The *ab inito* elastic constants for the C14 and C15 structures were derived from total energies as a function of suitably selected distortions. These energies were fitted to third-order polynomials from which the elastic constants at the equilibrium structures were calculated. It should be noted that in particular for the C14 structure a suitably large $\vec{k}$ points set of $12\times12\times10$ has to be taken into account in order to get reliably converged results.

The phonon dispersions and phonon densities of states for the C14 and C15 structures were derived by making use of the direct method[27–29] based on supercells with periodic boundary conditions. This approach relies on accurately calculated forces but is independent of the actual *ab initio* method. The forces are computed for independent displacements required by the symmetry of the unit cell. Displacement amplitudes of 0.03 Å were chosen. For the calculation of the force constants for the C14 and C15 structures the corresponding supercells contain 36 and 24 atoms, and a $3\times3\times3$ $\vec{k}$-point grid was applied. Phonon calculations were done for nonmagnetic as well as ferromagnetic cases.

TABLE I. *Ab initio* and experimental structural parameters for $ZrMn_2$ for the C14, C15, and C36 crystal structures considering nonmagnetic (NM), ferromagnetic (FM), and antiferromagnetic (AF) ordering. AF for C14 corresponds to AF2 (see text and Fig. 2). Lattice parameters a and c are given in angstroms, equilibrium volumes V_0 per formula unit in Å^3, and bulk moduli B in GPa.

Structure	a	c	V_0	B	Method
C14 NM	4.922	8.199	43.0	196	VASP
C15 NM	6.997		42.8	199	VASP
C36 NM	4.936	16.233	42.8	190	VASP
C14 FM	4.937	8.242	43.5	180	VASP
	5.026	8.258	45.2		Expt.[a]
	5.041	8.249	45.4		Expt.[b]
	5.046	8.295	45.3		Expt.[c]
	5.030	8.264	45.3		Expt.[d]
C15 FM	7.027		43.4	181	VASP
C36 FM	4.956	16.358	43.5	180	VASP
C14 AF	4.929	8.220	43.3	173	VASP
C15 AF	7.153		43.9	152	VASP
C36 AF	4.924	16.449	43.2		VASP

[a]Reference 6
[b]Reference 7
[c]Reference 8
[d]Reference 9

Finally, for the C14 and C15 structures we derived point defect properties for vacancies and antisite atoms. Supercells of 24 atoms for the C15 structure and 48 atoms for the C14 structure were constructed, and a $3\times3\times3$ $\vec{k}$-point grid was applied. The shape and volume of the supercells were kept fixed, whereas the atomic positions were allowed to relax. As reference energies the energies of formation of the compounds corresponding to the selected supercells were calculated. These energies served as input for a statistical mechanics model for deriving point defect properties within a grand canonical formulation.[30]

III. STRUCTURAL AND PHASE STABILITY

The ground-state structural parameters for $ZrMn_2$ with the C14, C15, and C36 crystal structures were obtained from the minimized total energies for nonmagnetic (NM), antiferromagnetic (AF), and ferromagnetic (FM) cases. For the C14 structure three different AF starting configurations were considered as described in Sec. II but we report only the results for the AF2 case (Fig. 2, right panel) because it is the energetically most stable antiferromagnetic phase. Therefore, from now on AF refers to the magnetic ordering as denoted by AF2. The lattice parameters are shown in Table I and the relaxed internal free parameters of atomic positions are listed in Table II for the C14 structure and in Table III for the C36 structure. For the cubic C15 structure there are no free coordinates due to its high symmetry. Experimentally, structural data are only available for the C14 structure. However, according to our calculations for the FM ground state the other

TABLE II. *Ab initio* calculated internal parameters of atomic positions for the C14 structure of NM, FM, and AF phases of $ZrMn_2$. AF corresponds to AF2.

Wyckoff parameter	NM	FM	AF
Zr: $4f(1/3,2/3,z)$	0.4365	0.4364	0.4360
Mn: $6h(x,2x,1/4)$	0.8301	0.8304	0.8292
Mn: $2a(0,0,0)$			

TABLE IV. *Ab initio* enthalpies of formation (kJ mol^{-1}) for nonmagnetic (NM), ferromagnetic (FM), and antiferromagnetic (AF) phases of $ZrMn_2$. For C14, the AF ordering corresponds to AF2.

	NM	AF	FM
C14	−56.8	−57.8	−60.6
C15	−51.5	−55.4	−60.9
C36	−55.2	−59.4	−60.7

two structures are energetically very close or even slightly lower, as already presented in our previous study.[18] The calculated volumes in Table I are all rather similar for the three structures in the NM and FM case. However, the AF results show a significantly larger volume for the C15 structure due to the *in-plane* antiferromagnetic ordering of the chosen model according to Nakamura *et al.* (Ref. 26). It might be possible that other AF structures (including noncollinear spin arrangements), which were not studied in this work, might have lower total energies. However, due to the rather small magnetic moments we do not expect any substantial change of our findings that ferromagnetism is the most stable magnetic ordering.

Comparing the calculated volumes for the energetically lowest FM results to the experimental data[2–8] we observe that the calculated data are smaller by about 4%, a deviation slightly larger than found for the nonmagnetic XCr_2 (X=Ti,Zr,Hf) compounds.[19] For the case of $ZrMn_2$, because of Mn, one could argue that the approximations to the exchange-correlation functional might be more in error when compared to the nonmagnetic Cr compounds. Note that in both cases we applied the same GGA functional but $ZrMn_2$ requires a spin polarized treatment. Furthermore, for $ZrMn_2$, measurements were done at elevated temperatures, and the samples are certainly off stoichiometric whereas our DFT results refer to T=0 K and perfect single crystals with perfect stoichiometry. The volume enhancing effect of magnetic pressure can be estimated by comparing the NM and FM data, and it appears to be less than 2%.

Energies of formation were derived in the standard way by the energy difference

$$\Delta H = U_{\mathrm{DFT}}(\mathrm{ZrMn_2}) - [U_{\mathrm{DFT}}(\mathrm{Zr}) + 2U_{\mathrm{DFT}}(\mathrm{Mn})] \quad (1)$$

of the corresponding DFT total energies U_{DFT} of the compounds and the pure elemental phases. The calculation for hexagonal close packed (hcp) Zr is straightforward but the ground state of solid Mn is extremely difficult to calculate because of the complicated magnetic ordering of α Mn.[31] One can, however, make use of the existence of the high-temperature γ Mn phase which can be quenched down to room temperature. The γ phase consists of antiferromagnetic layers in the [001] direction of a body-centered tetragonal (bct) structure, and can be easily calculated by a standard DFT approach. However, it should be noted that it is not clear how strongly localized the Mn d states are and if one has to go beyond standard DFT applications which we investigate at present.[32] For the present purpose we make use of the results of Hobbs *et al.*[31] because they also reported the energy difference for fcc γ Mn to α Mn, however, without relaxing the structure to bct. Including the fcc-bct relaxation energy from our calculations we calculated the energy difference between γ bct and α Mn to be 1.82 kJ mol^{-1}. By this procedure, enthalpies of formation for $ZrMn_2$ can be derived with respect to the (standard DFT) ground state of Mn. In a previous study on $TiMn_2$ (Ref. 33) we derived an energy of formation with respect to bct γ Mn of −88.8 kJ mol^{-1} which has now to be corrected to −85.2 kJ mol^{-1} when referring to α Mn. The corrected value is still in very good agreement to the experimental result[33] of −86.76±6.79 kJ mol^{-1}.

TABLE III. *Ab initio* calculated internal parameters of atomic positions for the C36 structure of NM, FM, and AF phases of $ZrMn_2$.

Wyckoff parameter	NM	FM	AF
Mn: $4f(1/3,2/3,z_1)$	0.1274	0.1247	0.1265
Mn: $6g(1/2,0,0)$			
Mn: $6h(x,2x,1/4)$	0.1621	0.1641	0.1620
Zr: $4e(0,0,z_2)$	0.0927	0.0934	0.0925
Zr: $4f(1/3,2/3,z_3)$	0.8437	0.8437	0.8434

Table IV presents the energies of formation (with respect to α Mn) for the equilibrium states of each structure and investigated magnetic ordering. As revealed in detail by Fig. 2 in Ref. 18 ferromagnetic spin polarization leads to a nearly degenerate sequence of formation energies: C15 is lowest but the two hexagonal structures C36 and C14 are less stable by only 0.2 to 0.3 kJ mol^{-1}. Such a structural degeneracy is characteristic for a polymorphic material. If, however, no magnetic ordering would occur C14 would be clearly the most stable phase, with the C15 phase higher up in energy by 5.3 kJ mol^{-1} according to Table IV.

Concerning the experimental energy of formation up to now only one result of −48.0 kJ mol^{-1} at high temperatures is reported.[34] Critical comparison with our significantly more negative value of −60.9 kJ mol^{-1} (lowest energy for C15 FM, see Table IV) cannot be made because the experiment is of limited reliability due to the application of a vapor pressure technique. In order to underline the quality of our approach we refer to the closely related (nonmagnetic) compound $TiMn_2$ for which we obtained very good agreement between our *ab initio* data and latest calorimetric measurements.[33] Clearly, new measurements of the energy of formation of $ZrMn_2$ are required.

Inspecting Fig. 2 of Ref. 18 and Table IV one realizes that the AF phases of the C14 and C36 structures are rather close

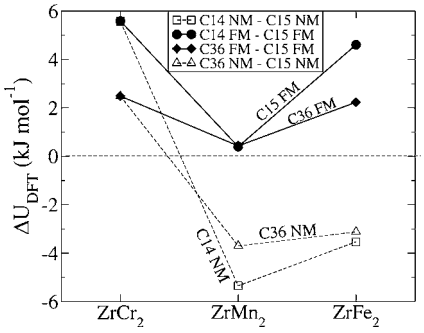

FIG. 1. Energy differences ΔU_{DFT} in kJ mol^{-1} between the C14 and C15 structures, and between the C36 and C15 structures for nonmagnetic (NM) and ferromagnetic (FM) phases of ZrX_2 (X =Cr,Mn,Fe) compounds. Positive values indicate that C15 is stable, negative values correspond to stable hexagonal structures.

in energy to the FM phases (higher only by 2.8 and 1.3 kJ mol^{-1}, respectively). The corresponding AF orderings are sketched in Fig. 2 showing also the local Mn moments. Because of the uncertainty concerning the proper treatment of the localization of Mn d states it is conceivable that effects of stronger correlation (i.e., going beyond standard DFT) could be of importance. As is well known then, when correlation is enhanced some suitable antiferromagnetic ordering may gain in energy with respect to ferromagnetic ordering, and depending on the strength of localization antiferromagnetism might then be even favored against ferromagnetism. Interestingly, up to now from experiment no clear indication of magnetic ordering was found for $ZrMn_2$. From our calculated results and considering possible stronger localization effects of the Mn d states one might speculate that a degeneracy between several magnetic states and crystal structures exists. In some sense this degeneracy might be related to the case of β Mn for which a spin-liquid state at very low temperatures was suggested.[35]

To illustrate the peculiar structural and magnetic behavior of $ZrMn_2$ Fig. 1 shows for $ZrCr_2$,$ZrMn_2$, and $ZrFe_2$ the structural competition between the cubic C15 and the two hexagonal structures depending on spin polarization, i.e., comparing NM and FM energy differences. For the nonmagnetic compound $ZrCr_2$, clearly C15 is stable. For the strongly magnetic compound $ZrFe_2$ (with Mn local moments larger than 2 μ_B) again C15 is stable but now because of magnetism. The NM result would clearly favor the C14 structure. $ZrMn_2$ is in between the two extreme cases with its rather small Mn moments of about 1 μ_B (see Table V) resulting in a peculiar structural degeneracy (and possibly—as discussed above—also in a magnetic degeneracy).

Comparing isovalent compounds, $TiMn_2$ is clearly of the C14 type with its electronic structure on the brink of spin polarization.[33] The magnetic properties of $HfMn_2$ concerning the local Mn moments are, according to our calculations, rather close to $ZrMn_2$, but for this compound the C14 FM phase is slighly more stable by 0.8 kJ mol^{-1} than the C15 FM phase. From the rather scarce experimental information on $HfMn_2$ the C14 is derived as the stable structure (at least at elevated temperatures[1]).

TABLE V. Local environment of Mn sites and distances d to nearest neighbors *nn* as well as averaged distance $\bar{d}$ in angstroms. Calculated local magnetic moments in μ_B and exchange splitting Δ in electron volts of Mn d-like states for the C14, C15, and C36 structures of ferromagnetic $ZrMn_2$.

Site	*nn*	d	$\bar{d}$	Magnetic moments	Δ
C14					
Mn(2a)	−6 Mn(6h)	2.51	2.51	1.24	1.26
	−6 Zr(4f)	2.89	2.89		
Mn(6h)	−2 Mn(2a)	2.51	2.48	0.60	0.62
	−2 Mn(6h)	2.42			
	−2 Mn(6h)	2.51			
	−4 Zr(4f)	2.90	2.91		
	−2 Zr(4f)	2.93			
C15					
Mn(16d)	−6 Mn(16d)	2.48	2.48	0.90	0.92
	−6 Zr(8a)	2.91	2.91		
C36					
Mn(4f)	−3 Mn(6g)	2.49	2.50	1.14	1.16
	−3 Mn(6h)	2.51			
	−3 Zr(4e)	2.91	2.91		
	−3 Zr(4f)	2.91			
Mn(6g)	−4 Mn(6g)	2.48	2.483	0.92	0.93
	−2 Mn(4f)	2.49			
	−4 Zr(4e)	2.91	2.916		
	−2 Zr(4f)	2.93			
Mn(6h)	−4 Mn(6h)	2.44	2.463	0.71	0.74
	−2 Mn(4f)	2.51			
	−4 Zr(4f)	2.91	2.913		
	−2 Zr(4e)	2.92			

IV. ELECTRONIC STRUCTURE AND MAGNETIC PROPERTIES

Table V lists the site and structure-dependent local magnetic moments as calculated for the Mn sites. The radius for deriving the local properties of Mn was chosen as 1.556 Å. In average the moments are in the order of 1 μ_B. However, they vary rather strongly depending on the local environment. For C15, because of high symmetry, there is only one Mn site and it has a moment of 0.90 μ_b for a Mn-Mn distance of 2.48 Å. The situation is quite different for the hexagonal C14 structure, for which we find two different moments, namely, 1.24 and 0.60 μ_B, significantly different when compared to the C15 environment. The larger moment arises for Mn(2a) sites of the C14 structure which have slightly larger nearest neighbor distances of 2.51 Å in comparison to the C15 distance of 2.48 Å. Although the increase in distance is rather small (about 1% for six neighbors) the influence on the magnetic moment is strong: it increases by 30%. This indicates how sensitive the magnetic properties of $ZrMn_2$ are with respect to small changes in the local environment. In contrast to the Mn(2a) site the moment of the Mn(6h) site is strongly reduced compared to C15 by 30%.

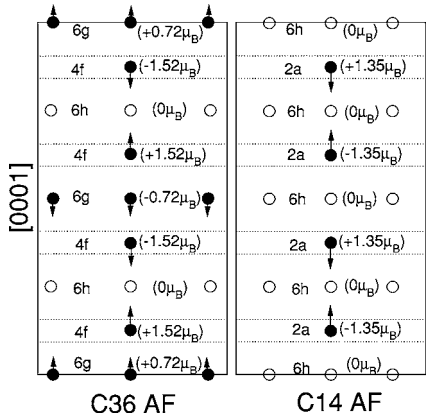

FIG. 2. Sketch of antiferromagnetic ordering of Mn moments in planes perpendicular to the [0001] direction for the hexagonal C36 and C14 structures of $ZrMn_2$. For C14 the AF ordering with lowest total energy was chosen (see text). Dashed lines indicate planes with Zr sites.

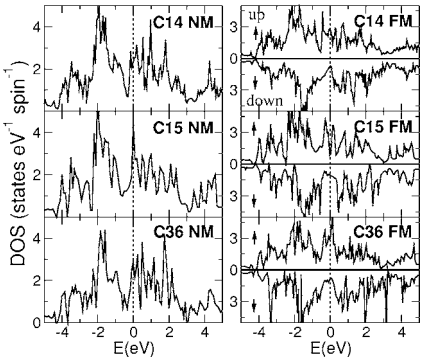

FIG. 3. Calculated total density of states (DOS) for the nonmagnetic (left panel) and spin resolved DOS for the ferromagnetically polarized (right panel) phases of the C14, C15, and C36 structures of $ZrMn_2$. Energy scale relative to Fermi energy.

This obviously is due to the rather short distance of 2.42 Å to two Mn(6*h*) neighbors which quenches the moment because of increased hybridization. This short distance to two Mn atoms seems to be of stronger influence for the local moment than the slightly enlarged distance of 2.51 Å for four other Mn neighbors. Inspecting the moments for C36 one finds three typical values for the magnetic moments, namely, a large one of 1.14 μ_B, a small one of 0.71 μ_B, and a rather unchanged one of 0.92 μ_B, when compared to the C15 structure. As discussed for the C14 structure the increase and decrease of moments can be analyzed in terms of increase and decrease of neighbor distances. Particularly striking is the short length of 2.44 Å for four of the Mn(6*h*)-Mn(6*h*) distances which quenches the local moment. The Zr local magnetic moments (not listed), which are antiparallel to the Mn moments, are in the range of −0.18 to −0.25 μ_B. So far no experimental evidence of magnetic ordering was reported for $ZrMn_2$.

Concerning the size of local moments for the C15 structure we find very good agreement with the *ab initio* results of Hong and Fu presented in Ref. 17. However, for C14 they report a value of 1.03 μ_B for the larger moment which is about 20% smaller than our result. Such a big difference cannot be attributed to different sphere sizes for calculating the local properties because otherwise the agreement with our calculated moments is good. It should be noted that for the C14 structure Hong and Fu applied a local density exchange-correlation functional whereas we applied a GGA functional for all cases. On the other hand, Hong and Fu seemed to have applied a GGA functional for the C15 structure.

As discussed in Sec. III according to our calculation antiferromagnetic (AF) phases with the C14 and C36 structures are energetically rather close to the ferromagnetic (FM) ground states. Therefore, we discuss the AF magnetic structure and local moments as shown in Fig. 2. As mentioned, for the C14 phase we only discuss the AF phase with the lowest energy. It consists of layers of Mn(2*a*) sites with alternating orientations of the moments, and—when compared to the FM phase—with a significantly larger moment of 1.35 μ_B. The Mn atoms in the 6*h* layers are magnetically dead presumably because of the symmetry of the AF arrangements of Mn(2*a*) moments. The result is more complicated for C36 for which we found a stable AF configuration with two different wavelengths of spin waves, a long wavelength of twice the unit cell dimension in [001] direction for Mn(6g) layers, and the second one for Mn(4*f*) sites of half the longer length. Again, Mn(6*h*) layers are magnetically dead. The moments of the Mn(4*f*) sites of 1.52 μ_B are strongly enhanced (compared to C15 FM) and twice as much as the moments of 0.72 μ_B for the longer spin wave.

The calculated total and partial density of states (DOS) are compiled in Figs. 3 and 4 for the nonmagnetic and ferromagnetic phases of all three structures. For the nonmagnetic cases (Fig. 3, left panel) the Fermi energy typically cuts into strongly uprising peaks resulting in values of the DOS at Fermi energy (E_F) which are so large that Stoner's instability criterion for spontaneous spin polarization is easily fulfilled and spin polarized ground states are derived (right panel). Table VI lists the DOS values at Fermi energy, clearly showing the large value for the nonmagnetic cases in particular for the high-symmetry C15 structure whereas for the hexagonal cases peaks are splitted due to the reduced symmetry. In comparison to XCr_2 (X=Ti,Zr,Hf) compounds,[19] for which E_F falls into the deep characteristic hybridization minimum of the DOS because of the smaller number of valence electrons, $d-d$ bonding states are now populated for $ZrMn_2$. This can be clearly seen in the features of the local DOS in Fig. 4 below E_F and above the characteristic minimum, which are of rather pure Mn d-like character.

The FM spin polarized DOS at $E_F n(E_F)$ in Fig. 4 shows a distinct and possibly important difference between the C14 structure (left panel) and the C15 structure (right panel). Whereas for the minority spin components the values for $n(E_F)$ are rather equally low, for the majority component the situation is different. For the C15 structure, E_F falls into a deep minimum between two peaks resulting in a low value for $n(E_F)$ illustrating the stabilizing effect of the spontaneous polarization. For the C14 structure $n(E_F)$ is still rather large which is due to Mn(2*a*) states indicating a possible instability although spin polarization was already achieved. This

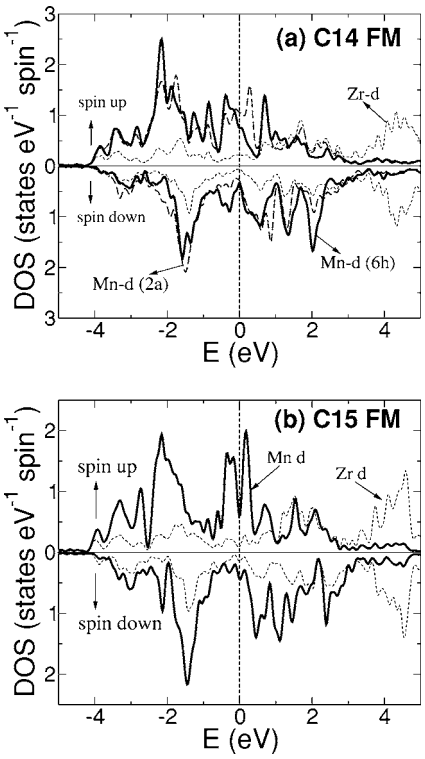

FIG. 4. Calculated site projected and spin resolved *d*-like local density of states (DOS) for the ferromagnetic phases of the C14 and C15 structures of $ZrMn_2$. Energy scale relative to Fermi energy.

might be a hint that stronger localization has to be considered, stronger than it is provided by the applied GGA functional. If that is the case, antiferromagnetic orderings (which even in our standard treatment are energetically close to the ferromagnetic ground state) could be more favorable.

In Fig. 4 some small spin splitting is found for Zr *d*-like states which results in small magnetic moments antiparallel to the Mn moments.

V. ELASTIC PROPERTIES

The elastic constants of $ZrMn_2$ were calculated for the NM as well as the FM phases in the C14 and C15 crystal structures. The results as presented in Table VII do not show any elastic instability[36] which confirms our prediction of polymorphism,[18] i.e., the coexistence of several *stable* crystal structures. In comparison to the calculated results for the nonmagnetic $ZrCr_2$ compound with C15 structure[19] the elastic constants for the FM C15 phase of $ZrMn_2$ are rather similar apart from a rather low value of the shear constant of $c_{44}=21$ GPa. For $ZrMn_2$ in general, the values for the bulk moduli are about 180 GPa for the FM structures and about 200 GPa for the NM structures. The smaller values for the ferromagnetic cases is due to their slightly larger equilibrium volumes as shown in Table VII. A noticeable difference between the elastic properties of NM and FM C15 $ZrMn_2$ is expressed by c' which reflects the rigidity against volume conserving tetragonal distortions. The much larger value of $c'=50$ GPa for the FM case indicates stabilization against tetragonal distortions when compared to the energetically much less favorable NM case. For describing anisotropic elastic properties the so-called elastic anisotropy ratio $A=2c_{44}/(c_{11}-c_{12})$ is calculated. For C15 $ZrMn_2$ in the NM case it amounts to 2.24 whereas it is strongly reduced to 0.42 for the FM compound. These anisotropy ratios are very unusual when compared to known values for other C15 Laves phases: NM $ZrMn_2$ has the largest value of A, whereas for the FM case it is the smallest value. The strong reduction of A for the FM phase of $ZrMn_2$ when compared to the NM case indicates that spin polarization makes the bonding more anisotropic.

To complete the study about the elastic constants some important polycrystalline elastic moduli and the Debye temperatures are presented in Table VIII. For that, the single crystalline elastic constants were used within Hill's average for randomly oriented crystallites. To our knowledge, no experimental data for the elastic properties of $ZrMn_2$ have been published so far. Therefore, our calculated data shown in Tables VII and VIII are pure predictions awaiting experimental confirmation.

TABLE VI. Calculated density of states at E_F for spin resolved DOS $n_\uparrow(E_F)$ and $n_\downarrow(E_F)$ in states eV^{-1} f.u.$^{-1}$ spin^{-1}. Total DOS at E_F $n_{tot}(E_F)$ for spin polarized and $n_{tot}^{NM}(E_F)$ for nonmagnetic phases in eV^{-1} f.u^{-1} and specific heat γ (defined as $C_{el}/T=1/3n(E_F)\pi^2k_B^2$) in mJ mol^{-1} K^{-2} for the C14, C15, and C36 structures of $ZrMn_2$.

	C14	C15	C36
$n_\uparrow(E_F)$	2.31	0.83	3.01
$n_\downarrow(E_F)$	0.78	1.04	0.84
$n_{tot}(E_F)$	3.09	1.87	3.85
$n_{tot}^{NM}(E_F)$	5.16	8.25	5.54
γ (FM)	7.3	4.4	9.1
γ (NM)	12.2	20.0	13.06

TABLE VII. *Ab initio* elastic constants in GPa at the calculated equilibrium volumes for the NM and FM phases of the C14 and C15 structures of $ZrMn_2$. Also shown are the shear moduli $c'=1/2(c_{11}-c_{12})$ for C15 and $c_{66}=1/2(c_{11}-c_{12})$ for C14, and the bulk moduli as derived from the elastic constants. The values denoted by (B) are derived from volume derivatives of the volume dependent total energies.

	c_{11}	c_{12}	c_{44}	c'	B		
C15 NM	219	186	37	17	197 (199)		
C15 FM	250	150	21	50	184 (181)		
	c_{11}	c_{12}	c_{13}	c_{33}	c_{44}	c_{66}	B
C14 NM	240	192	155	279	37	24	195 (196)
C14 FM	231	196	132	269	50	18	181 (180)

VI. VIBRATIONAL PROPERTIES

As discussed in our recent study reporting the polymorphic properties of $ZrMn_2$ (Ref. 18) the entropy contribution

TABLE VIII. *Ab initio* polycrystalline elastic moduli derived from the elastic constants at the calculated equilibrium volumes. The symbols $E, G, \nu, \upsilon_m, \Theta_D$ refer to Young's modulus, shear modulus (all in units of GPa), Poisson's ratio, average sound velocity (in m s^{-1}), and Debye temperature (in Kelvin), respectively.

	E	G	ν	υ_m	Θ_D
C15 NM $ZrMn_2$	77	27	0.43	1943.3	239
C15 FM $ZrMn_2$	85	30	0.42	2068.7	253
C14 NM $ZrMn_2$	106	38	0.41	2496.0	305
C14 FM $ZrMn_2$	120	43	0.39	2678.3	327

to the phonon free energy is the driving force for a structural phase transition from the FM C15 structure to the FM C14 structure at about 160 K. The equations for deriving the phonon free energy from the phonon DOS are given in Ref. 19. In the present study for $ZrMn_2$ we present the detailed results of the phonon dispersions and density of states (DOS) for the FM C15 and C14 phases in Fig. 5 as well as for the corresponding NM phases in Fig. 6.

Comparing the NM and FM phases a clear distinction is found concerning the width of the DOS. For the NM phase the DOS for both structures are significantly broadened due to the occurrence of rather low-frequency branches with weak dispersion at about 2 THz indicating softening and weakening of bonding as compared to the FM phases. In the FM case the onset of these branches starts at about 3.5 THz. This is another indication of the stability of the FM phases. This distinct difference between NM and FM phases could serve as a check if $ZrMn_2$ orders ferromagnetically or not.

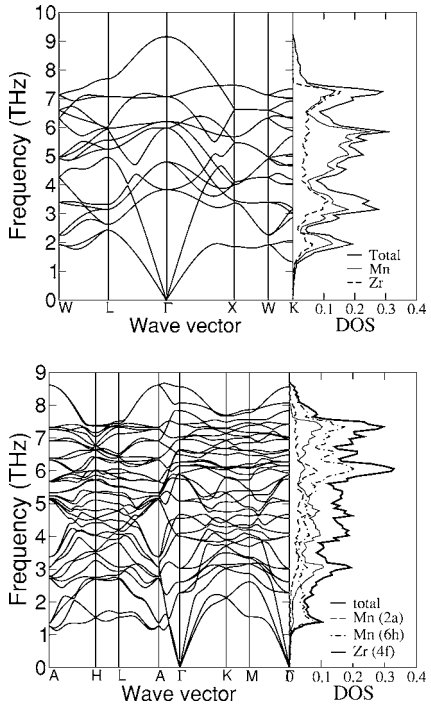

FIG. 5. *Ab initio* phonon dispersion relations and total and partial densities of states for nonmagnetic $ZrMn_2$ in the C15 (upper panel) and C14 (lower panel) structure.

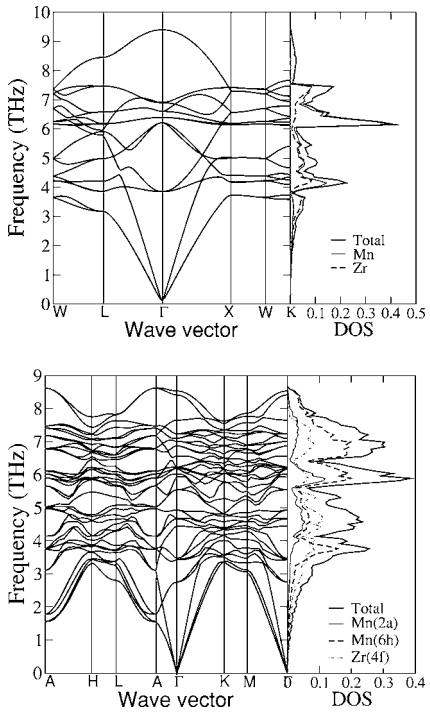

FIG. 6. *Ab initio* phonon dispersion relations and total and partial densities of states for ferromagnetic $ZrMn_2$ in the C15 (upper panel) and C14 (lower panel) structures.

We hope that future experiments for the vibrational properties will clarify this point.

The decomposition of the DOS into characteristic Mn- and Zr-like contributions reveals three different frequency ranges: for the FM phase a low frequency range between 3 and 6 THz (2.3 to 4 THz for the NM phase); a rather pure Mn-like peak between 6 and 7 THz (4 to 6.5 THz for NM); and a high frequency range from 7 to 7.5 THz (or 6.5 to 8 THz for NM).

Because of differences in symmetry there are many more branches for the C14 structures as compared to C15 since the C14 unit cell contains 12 atoms and the C15 cell 6 atoms. Comparing the FM phases, for the C14 structure one observes low frequency states of about 2 THz at point A, whereas nothing like this is to be seen for the C15 structure. Because of the strong dispersion of these bands starting at point A the contribution to the DOS is very small. Nevertheless, experiments focusing on this particular point in reciprocal space could reveal important information about the structure.

In all cases, all phonon frequencies are real and no complex frequencies indicating instabilities are observed (even for the softer NM phases). This is of importance for the proposed coexistence of stable polymorphic structures.

For the FM C14 and C15 phases focusing on the calculated vibrational internal energies [Fig. 6(b), left panel] we derive very similar zero point energies of 10.0 and 9.8 kJ mol^{-1} for the C15 and C14 structures, respectively. Increasing temperature, the vibrational internal energy further stabilizes the C15 structure. However, the by far dominating part of the vibrational free energy is the vibrational entropy which drives a structural transition from C15 to C14.

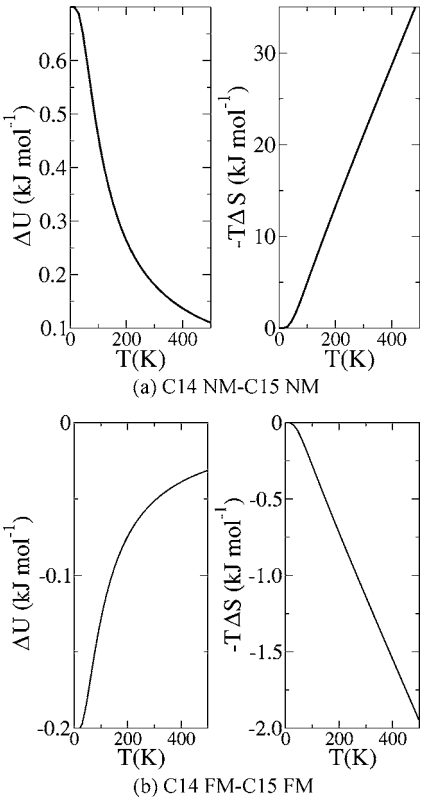

FIG. 7. Temperature dependence of the structural difference C14 minus C15 of the *ab initio* vibrational free energies decomposed into internal energy and entropy contributions for the nonmagnetic (a) and ferromagnetic (b) phases of $ZrMn_2$.

In our recent study[18] we claimed a critical temperature of $T_{tr}(\mathrm{FM})=160$ K for this transition. A numerically more elaborate calculation was made in the present study yielding a slightly increased value of $T_{tr}(\mathrm{FM})=200$ K. As derived from these phonon calculations, for the FM case in Fig. 7(b) the gain in entropy for C14 at $T_{tr}(\mathrm{FM})$ is sufficient to compensate the very small structural stabilization energy of 0.1 kJ mol^{-1} of the C15 structure at $T=0$ K. The value of 0.1 is the result of the differences of the DFT energies and the zero point energies. With increasing temperature the vibrational entropy increasingly favors the C14 structure which is found experimentally.

The structural competition as derived from the calculated vibrational properties for the NM phases is entirely different from the FM case. For the NM study the zero point energies for C14 and C15 are now 9.3 and 8.6 kJ mol^{-1}, respectively. In combination with the DFT energy difference $\delta U_{\mathrm{DFT}}=U_{\mathrm{DFT}}(\mathrm{C14})-U_{\mathrm{DFT}}(\mathrm{C15})=-5.3$ kJ mol^{-1} (Table IV) the structural internal energy difference of −4.6 kJ mol^{-1} favors C14 at $T=0$ K. The temperature dependence of both vibrational internal energy and vibrational entropy differences as shown in Fig. 7(a) behaves in just the opposite way as it did for the FM phases in Fig. 7(b). Whereas with increasing temperature the internal energy contribution slightly increases the stability of the C14 phase, the entropy contribution favors the C15 structure very strongly. As a matter of fact, both quantities have the same temperature dependent trend as derived for the nonmagnetic compound $ZrCr_2$.[19]

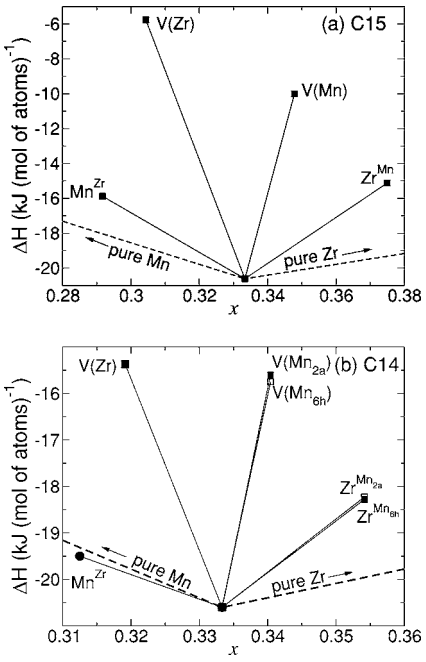

FIG. 8. *Ab initio* enthalpies of formation for compounds Zr_xMn_{1-x} as obtained from defect supercells versus the concentration x of Zr atoms for the C15 structure (upper panel) and the C14 structure (lower panel). V(Zr): vacancy at Zr site, V(Mn): vacancy at Mn ($2a$) and ($6h$) sites, Zr^{Mn}: Zr at the Mn ($2a$) and ($6h$) sites, Mn^{Zr}: Mn at Zr site.

However, it should be noticed that the energy scale of the entropy difference for NM $ZrMn_2$ is much larger than for both compounds, $ZrCr_2$ as well as FM $ZrMn_2$. This temperature dependence has a consequence: If $ZrMn_2$ would be a nonmagnetic material, then above a temperature of $T_{tr}(\mathrm{NM})\approx 850$ K the C15 structure would become stable. At this temperature the internal energy difference of −4.6 kJ mol^{-1} at $T=0$ K is compensated by the vibrational entropy contribution to the free energy, and the C15 structure would be increasingly favored for temperatures above $T_{tr}(\mathrm{NM})$. This finding disagrees with experiment because the C14 structure was found to be stable up to the melting point. Up to now no reliable experimental evidence for any magnetic state of $ZrMn_2$ is available.

VII. POINT DEFECTS

The energetics of formation of point defects were calculated within a supercell approach as applied in Ref. 19. In particular, vacancies V(Zr) at the Zr and V(Mn) at the Mn sites, and antisite defects Zr^{Mn} for Zr occupying a Mn site and Mn^{Zr} for Mn occupying a Zr site were considered. Because of symmetry this results in four possible point defects for C15, and in six different point defects for the C14 structure due to the crystallographically inequivalent ($2a$) and ($6h$) sites occupied by Mn atoms.

The enthalpies of formation for Zr_xMn_{1-x} compounds as calculated from the total energies of the supercells are summarized in Fig. 8. For both structures clearly the formation of antisites is preferred when compared to vacancies, and the

TABLE IX. Calculated defect formation energies for the C14 and C15 structures of ferromagnetic $ZrMn_2$ at 1500 K as derived from a statistical mechanics model (see text).

	V(Mn)	V(Zr)	Mn^{Zr}	Zr^{Mn}
C15	2.64	3.74	1.19	1.19
C14	2.53	2.96	0.89	0.89

Mn^{Zr} antisite defects are the most favorable ones. This might qualitatively be understood by simple arguments based on atomic sizes disregarding the change in bonding when Mn replaces a Zr atom: Since Mn atoms are considered to be smaller than Zr atoms, Mn easily fits into Zr sites. For the C14 compound the formation energy of the supercell with a Mn^{Zr} defect is so low that by 0.2 kJ (mol of atoms)$^{-1}$ it falls below the dashed line in Fig. 8 marking the boundary of thermodynamic stability connecting the formation energy of defect-free $ZrMn_2$ and zero (pure Mn). This indicates that the ordered compound with the supercell structure for the Mn^{Zr} defect is energetically more stable than a mixture of pure Mn and $ZrMn_2$ which seems to be unphysical. Since this unexpected result is reliable—as it was carefully checked—it strongly indicates (i) the possible existence of other ordered Zr-Mn compounds with Mn concentrations larger than 2/3 and (ii) a broadening of the homogeneity range of $ZrMn_2$ towards Mn-rich compositions, as discussed in the following paragraph. However, up to now for the Zr-Mn phase diagram only the compound $ZrMn_2$ is reported to exist. Further experimental studies on the Mn-rich part of the phase diagram are thus encouraged by our *ab initio* results.

An appropriate description of point defects is based on the ordered compound $ZrMn_2$ as a reference and suitable chemical potentials describing the variation of stoichiometry within a statistical mechanics model based on the grand canonical ensemble.[30] It is noted, however, that in particular at higher temperatures complicated defect combinations may significantly contribute to the configurational entropy. Furthermore, vibrational effects are not included. The discussed procedure is the same as used for our study on $ZrCr_2$.[19]

Table IX lists the defect formation energies at 1500 K for the stoichiometric composition. Antisite defects are again found to be the preferred defects in $ZrMn_2$. Within the statistical model temperature-dependent defect concentrations can be derived. Defect concentrations for temperatures from 500 to 1500 K are listed in in Table X, emphasizing again the dominance of antisite defects.

TABLE X. Calculated temperature-dependent defect concentrations for ferromagnetic and stoichiometric $ZrMn_2$ in the C14 and C15 crystal structures.

	C15			C14		
T(K)	V(Mn)	V(Zr)	Anti	V(Mn)	V(Zr)	Anti
500	2.6*E*-27	1.8*E*-38	1.0E-12	2.7*E*-28	1.4*E*-30	1.1*E*-09
1000	5.1*E*-14	1.4*E*-19	1.0E-06	1.6*E*-13	1.2*E*-15	3.3*E*-05
1500	3.7*E*-09	2.6*E*-13	1.0E-04	3.0*E*-09	1.1*E*-10	1.0*E*-03

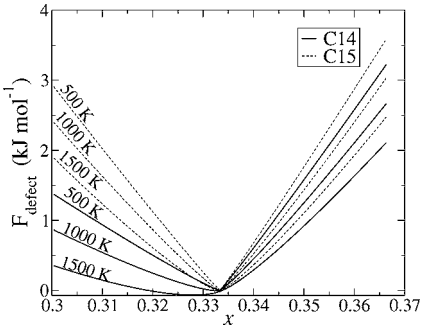

FIG. 9. Temperature-dependent defect free energy fo Zr_xMn_{1-x} for the ferromagnetic C14 (solid lines) and C15 (dashed lines) phases.

Based on the statistical model the temperature-dependent free energies of C14 and C15 $ZrMn_2$ were calculated and are presented in Fig. 9. With increasing temperature the minimum of the free energy of C14 $ZrMn_2$ does not any more occur at the stoichiometric composition $x=33.3$ at. % but is shifted toward Mn-richer compositions. At 1500 K the minimum of the free enery is already found for a composition of $x=32.8$ at. %. This implies that also the congruent melting point may not occur at the stoichiometric composition but at the Mn-rich side. In addition it is anticipated that Mn antisites may produce a broad nonstoichiometry range toward the Mn-rich side, in agreement with the experimental phase diagram. It is well known, that $ZrMn_2$ samples produced by the standard melting techniques are off stoichiometric with a slightly enriched Mn concentration.

Finally, the change of magnetic moments upon defect formation is investigated. A very striking effect is observed for the Mn antisite Mn^{Zr} defect which is also the dominant defect type at Mn-richer compositions: The local moment of the Mn atom increases from about 1 μ_B for the defect-free compound $ZrMn_2$ to 3.2 μ_B for the Mn^{Zr} defect, for both the C14 and C15 structures (see Table XI). This massive increase of the magnetic moments is due to the change in local coordination: Compared to the defect-free compound the Mn defect atom at a Zr site has significantly increased nearest neighbor distances to the surrounding Mn atoms causing an enhanced localization of the Mn states which results in a

TABLE XI. Local magnetic moments $m(\mu_B)$ of the Mn^{Zr} defect at Zr sites, and of atoms at nearest neighbor (NN) sites with distances d (Å) from the defect. Compare with Table V for local moments in defect-free $ZrMn_2$.

Defect	NN	d	m
C14 Mn^{Zr}			3.22
	−3 Mn	2.85	1.13
	−6 Mn	2.86	0.54
	−3 Mn	2.93	0.72
	−4 Zr	2.94	−0.23
C15 Mn^{Zr}			3.21
	−12 Mn	2.95	0.79
	−4 Zr	2.94	−0.19

strong increase of its local moment. The local moments of the nearest neighbor Mn and Zr atoms around the antisite Mn atom are only slightly changed with respect to the defect-free structure (Table XI). Experiments should be able to detect the predicted large magnetic moments of Mn^{Zr} which -in reality- might appear as disordered local moments.

VIII. SUMMARY AND CONCLUSION

From experimental studies at elevated temperatures, $ZrMn_2$ has been characterized as crystallizing in the hexagonal C14 crystal structure. The experimental Zr-Mn phase diagram contains $ZrMn_2$ as the only existing compound within the whole composition range. Little is known about phase and structural stabilities at low temperatures. Furthermore, up to now no experimental data about the existence of any magnetic phase or local magnetic moments have been reported.

In our *ab initio* density functional study on $ZrMn_2$, a range of ground-state properties are investigated for the most common crystal structures of Laves phase compounds, namely, for the the cubic C15 and the hexagonal C14 and C36 structures.

From the density functional energies structure-dependent formation energies were derived which—due to the standard density functional approach—refer to very low temperatures. Particular emphasis was put on the search for magnetic ground-state phases by investigating ferromagnetic and several antiferromagnetic spin arrangements. We found that a ferromagnetic phase with the C15 structure is lowest in energy. However, the corresponding ferromagnetic C14 and C36 structures have formation energies which are very close to the C15 phase being less stable by only 0.3 and 0.2 kJ mol^{-1}, respectively. This structural energy degeneracy indicates a possible polymorphism for $ZrMn_2$. The occurrence of spin polarization is clearly manifested already in the nonmagnetic electronic structures because of the fulfillment of Stoner's instability criterion. Compared to the ferromagnetic results, nonspin-polarized calculations yield totaly different structural stabilities, the C14 structure being the most favorable one and lower in energy by about 5 kJ mol^{-1} than the corresponding energy for the C15 structure. The gain in formation energy, i.e., the strengthening of bonding due to ferromagnetic spin polarization is 4 and 9 kJ mol^{-1} for the C14 and C15 structures, respectively.

Studying the magnetic phases in more detail, it is found that the local Mn moments being in the order of 1 μ_B for the C15 structure are rather sensitive to changes of the local environment: For the hexagonal phases the Mn moments are either increased or decreased by about 30% at the respective hexagonal sites. Furthermore, it was found that some of the antiferromagnetic phases are energetically rather close to the ferromagnetic ground states. One might therefore speculate that a possible degeneracy of ferro- and antiferromagnetic phases might occur if the treatment of the Mn *d* states needs to be corrected for stronger localization. Stronger correlation usually favorizes antiferromagnetic spin orderings. Experimentally, up to now nothing is known about a possible magnetic phase of $ZrMn_2$.

A further clear indication for magnetic ordering in $ZrMn_2$ is provided by comparison of elastic properties calculated for nonmagnetic and ferromagnetic phases. For the nonmagnetic C15 phase a rather small value of 17 GPa for the c' parameter representing tetragonal distortions and an unusually large value for the anisotropy ratio A of 2.24 is obtained. Both parameters indicate a rather soft material, in particular with respect to tetragonal strains. The onset of ferromagnetism increases c' to as much as 50 GPa and the anisotropy ratio is strongly reduced to 0.42, thus remarkably stabilizing the ferromagnetic compound with respect to tetragonal shears.

Addressing the question, whether the calculated ferromagnetic C15 ground state at $T=0$ K could be in accordance with the experimentally observed C14 phase at elevated temperatures, the temperature-dependent vibrational free energy was calculated from the *ab initio* phonon dispersions for the nonmagnetic and ferromagnetic phases with the C14 and C15 structures. For the ferromagnetic phases it turns out that the vibrational entropy contribution to the free energy difference strongly favors the ferromagnetic C14 phase at higher temperatures, causing a structural transition from C15 to C14 at a critical temperature of $T_{tr}(\mathrm{FM})=200$ K. On the other hand considering nonmagnetic phases, the stable C14 structure at $T=0$ K is transformed into a C15 phase at $T_{tr}(\mathrm{NM})=850$ K, and C15 is even more stabilized with increasing temperature which is in contradiction to the experimental findings of a stable C14 structure up to the melting point. Therefore, the *ab initio* thermodynamics of ferromagnetic phases is consistent with experimental high temperature observations, whereas for non-magnetic phases it is not. This result provides yet another indication for some magnetic ordering.

By combining a supercell approach with a statistical mechanics model defect formation properties for the ferromagnetic C14 and C15 phases are calculated. As a result of the supercell calculations we predict that some ordered compounds with a Mn concentration larger than 2/3 may exist which is yet not confirmed experimentally. According to our data Mn antisite atoms at the Zr sublattice are the dominant defects, which causes a broad homogeneity range of the $ZrMn_2$ phase toward the Mn richer side of the phase diagram, in accordance with experiment. Another striking result was obtained when studying the magnetic moments of the defect structures. The Mn antisite atoms exhibit large magnetic moments of more than 3 μ_B which should be detectable by experiment in terms of disordered local moments.

In conclusion, our study on formation energy, free energy, elastic and vibrational properties, and defect formation of the Laves-phase compound $ZrMn_2$ provides a strong indication that some kind of magnetic ordering exists which has yet not been verified experimentally. For verification, experimental investigations of elastic constants and phonon frequencies in selected areas of the Brillouin zone are suggested. Magnetic moments in the vicinity of Mn antisite defects should be detectable. A search for possible ordered Mn-rich phases is suggested. At low temperatures, a degeneracy of at least three magnetic structures is predicted, representing low temperature polymorphism.

ACKNOWLEDGMENTS

Helpful discussions with A. Grytsiv, M. Rotter, and E. Bauer are appreciated. This work was supported by the Austrian Science Fund FWF Project No. P16957. Most of the calculations were performed on the Schrödinger-2 PC cluster of the University of Vienna. X.Q.C. is grateful to the OEAD for support within the Austrian Chinese Technical Scientific Exchange Program, Project No.VII.A.16.

[1] V. N. Svechnikov and V. V. Pet'kov, Metallofizika (Kiev) (Akademiya nauk ukrainskoi SSR, Institute Metallofiziki) **64**, 24 (1976).
[2] T. B. Massalski, H. Okamoto, P. R. Subramanian, and L. Kacprozak, in *Binary Alloys Phase Diagrams*, edited by T. B. Massalski, H. Okamoto, P. R. Subramanian, and L. Kacprozak (The Materials Information Society, ASM International, 1989), Vol. 3, p. 2629.
[3] R. M. van Essen and K. H. J. Bushow, Mater. Res. Bull. **15**, 1149 (1980).
[4] L. Y. Zhang, A. T. Pedziwatr, F. Pourarian, and W. E. Wallace, J. Magn. Magn. Mater. **68**, 309 (1987).
[5] F. Pourarian, H. Fujii, W. E. Wallace, V. K. Sinha, and H. K. Smith, J. Phys. Chem. **85**, 3105 (1981).
[6] V. K. Sinha and W. E. Wallace, J. Less-Common Met. **106**, 199 (1985).
[7] Ž. Blažina and R. Trojko, J. Less-Common Met. **133**, 277 (1987).
[8] H. Flandorfer, J. Cröbner, A. Stamou, N. Hassiotis, A. Saccone, P. Rogl, R. Wouters, H. Seifert, D. Maccio, R. Ferro, G. Haidemenopoulos, L. Delaey, and G. Effenberg, Z. Metallkd. **88**, 529 (1997).
[9] L. D. Gulay and V. I. Zaremba, J. Alloys Compd. **347**, 184 (2002).
[10] I. I. Bulyk, Yu. B. Basaraba, and A. M. Trostianchyn, J. Alloys Compd. **367**, 283 (2004).
[11] T. M. Shavishvili, A. I. Meskhishvili, and T. D. Andriadze, Fiz. Met. Metalloved. **47**, 880 (1979) , [Phys. Met. Metallogr. **47**, 880 (1979)].
[12] I. Jacob, D. Davidov, and D. Shaltiel, J. Magn. Magn. Mater. **20**, 226 (1980).
[13] S. Ishida, S. Asano, and J. Ishida, J. Phys. Soc. Jpn. **54**, 3925 (1985).
[14] S. Asano and S. Ishida, J. Magn. Magn. Mater. **70**, 39 (1987).
[15] T. Matsumura, H. Yukawa, and M. Morinaga, J. Alloys Compd. **279**, 192 (1998).
[16] H. Yamada, Physica B & C **149**, 390 (1988).
[17] S. Hong and C. L. Fu, Phys. Rev. B **66**, 094109 (2002).
[18] X. Q. Chen, W. Wolf, R. Podloucky, P. Rogl, and M. Marsman, Europhys. Lett. **64**, 807 (2004).
[19] X. Q. Chen, W. Wolf, R. Podloucky, and P. Rogl, Phys. Rev. B **71**, 174101 (2005).
[20] G. Kresse and J. Furthmüller, Comput. Mater. Sci. **6**, 15 (1996); , Phys. Rev. B **54**, 11169 (1996).
[21] P. E. Blöchl, Phys. Rev. B **50**, 17953 (1994).
[22] G. Kresse and D. Joubert, Phys. Rev. B **59** 1758 (1999).
[23] J. P. Perdew and Y. Wang, Phys. Rev. B **45**, 13244 (1992).
[24] S. H. Vosko, L. Wilk, and M. Nusair, Can. J. Phys. **58**, 1200 (1980).
[25] H. J. Monkhorst and J. D. Pack, Phys. Rev. B **13**, 5188 (1976).
[26] H. Nakamura, N. Metoki, S. Suzuki, F. Takayanagi, and M. Shiga, J. Phys.: Condens. Matter **13**, 475 (2001).
[27] W. Frank, C. Elsässer, and M. Fähnle, Phys. Rev. Lett. **74**, 1791 (1995).
[28] G. Kresse, J. Furthmüller, and J. Hafner, Europhys. Lett. **32**, 729 (1995).
[29] K. Parlinski, *Software Phonon 3.11 (2002)* as implemented in MedeA, Materials Design s.a.r.l. (2003), www.materialsdesign-.com; K. Parlinski, Z-.Q. Li, and Y. Kawazoe, Phys. Rev. Lett. **78**, 4063 (1997).
[30] B. Meyer and M. Fähnle, Phys. Rev. B **59**, 6072 (1999). **60**, 717 (1999); M. Rasamny, M. Weinert, G. W. Fernando, and R. E. Watson, *ibid.* **64**, 144107 (2001).
[31] D. Hobbs, J. Hafner, and D. Spišák, Phys. Rev. B **68**, 014407 (2003); J. Hafner and D. Hobbs, *ibid.* **68**, 014408 (2003).
[32] X. Q. Chen, C. Franchini, A. Filippetti, and R. Podloucky (unpublished).
[33] X. Q. Chen, V. T. Vitusiewicz, R. Podloucky, P. Rogl, and F. Sommer, Acta Mater. **51**, 1239 (2003).
[34] F. Smetana, P. Entner, and A. Neckel, Monatsch. Chem. **101**, 956 (1970).
[35] J. R. Stewart, B. D. Rainford, R. S. Eccleston, and R. Cywinski, Phys. Rev. Lett. **89**, 186403 (2002).
[36] J. F. Nye, in *Physical Properties of Crystals* (Clarendon Press, Oxford, 1985), p. 142.